書籍

著者氏名	論文タイトル名	書籍全体の編集者名	書 籍 名	出版社名	出版地	出版年	ページ
Tanaka, K. Yashiroda, H., and Murata, S. (2005)	Ubiquity and diversity of the proteasome system.	Mayer, R. J., Ciechanover, A., and Rechsteiner, M.	Protein Degradation	Wiley-VCH Verlag GmbH	Weinheim, Germany	2005	In press
田中啓二	概論・ユビキチンの発見物語	田中啓二(編集)	ユビキチンがわかる(わかる実験医学シリーズ)	羊土社	東京	2004	16-23

雑誌

発表者氏名	論文タイトル名	発表誌名	巻号	ページ	出版年
Ishigaki, S., Hishikawa, N., Niwa , J., Iemura, S., Natsume , T., Hori, S.,Kakizuka, A., Tanaka, K., and Sobue, G.	Physical and functional interaction between Dorfin and VCP that are colocalized in ubiquitylated inclusions in neurodegenerative disorders.	J. Biol. Chem	279	51376-51385	2004
Mizushima, T., Hirao, T., Yoshida, Y., Lee, S. J., Chiba, T., Iwai, K., Yamaguchi, Y., Kato, K., Tsukihara, T., and Tanaka, K.	Structural basis of sugar-recognizing ubiquitin ligase.	Nature Struct.& Mol. Biol.	11	365-370	2004
Tenno, T., et al.	Structural basis for distinct roles of Lys 63- and Lys 48-linked polyubiquitin chains	Genes to Cells	10	865-875	2004

研究成果の刊行物・別冊

doi:10.1093/brain/awh381 *Brain* (2005), **128**, 659–670

Widespread nuclear and cytoplasmic accumulation of mutant androgen receptor in SBMA patients

Hiroaki Adachi,[1] Masahisa Katsuno,[1] Makoto Minamiyama,[1] Masahiro Waza,[1] Chen Sang,[1] Yuji Nakagomi,[2] Yasushi Kobayashi,[1] Fumiaki Tanaka,[1] Manabu Doyu,[1] Akira Inukai,[1] Mari Yoshida,[3] Yoshio Hashizume[3] and Gen Sobue[1]

[1]*Department of Neurology, Nagoya University Graduate School of Medicine, Nagoya,* [2]*Central Research Laboratories, School of Medicine, Aichi Medical University and* [3]*Department of Neuropathology, Institute for Medical Sciences of Aging, Aichi Medical University of Aichi, Japan*

Correspondence to: Gen Sobue, MD, PhD, Department of Neurology, Nagoya University Graduate School of Medicine, 65 Tsurumai-cho Showa-ku, Nagoya, 466-8550, Japan
E-mail: sobueg@med.nagoya-u.ac.jp

Summary

Spinal and bulbar muscular atrophy (SBMA) is an inherited adult onset motor neuron disease caused by the expansion of a polyglutamine (polyQ) tract within the androgen receptor (AR), affecting only males. The characteristic pathological finding is nuclear inclusions (NIs) consisting of mutant AR with an expanded polyQ in residual motor neurons, and in certain visceral organs. We immunohistochemically examined 11 SBMA patients at autopsy with 1C2, an antibody that specifically recognizes expanded polyQ. Our study demonstrated that diffuse nuclear accumulation of mutant AR was far more frequent and extensive than NIs being distributed in a wide array of CNS nuclei, and in more visceral organs than thus far believed. Mutant AR accumulation was also present in the cytoplasm, particularly in the Golgi apparatus; nuclear or cytoplasmic predominance of accumulation was tissue specific. Furthermore, the extent of diffuse nuclear accumulation of mutant AR in motor and sensory neurons of the spinal cord was closely related to CAG repeat length. Thus, diffuse nuclear accumulation of mutant AR apparently is a cardinal pathogenetic process underlying neurological manifestations, as in SBMA transgenic mice, while cytoplasmic accumulation may also contribute to SBMA pathophysiology.

Keywords: polyglutamine; spinal and bulbar muscular atrophy; diffuse nuclear accumulation; nuclear inclusion, cytoplasmic accumulation

Abbreviations: polyQ = polyglutamine; SBMA = spinal and bulbar muscular atrophy; AR = androgen receptor; NIs = nuclear inclusions; DRPLA = dentatorubral-pallidoluysian atrophy; CBP = CREB-binding protein

Received June 15, 2004. First revision August 23, 2004. Second revision November 26, 2004. Accepted November 30, 2004. Advance Access publication January 19, 2005

Introduction

Polyglutamine (polyQ) diseases are inherited neurodegenerative disorders caused by expansion of a trinucleotide CAG repeat in the causative genes. To date, nine polyQ diseases have been identified (Ross, 2002). Spinal and bulbar muscular atrophy (SBMA) is a polyQ disease involving mainly spinal and brainstem motor neurons (Kennedy *et al.*, 1968; Sobue *et al.*, 1989). In SBMA, a polymorphic CAG repeat ordinarily consisting of 14–32 CAGs is expanded to 40–62 CAGs in the first exon of the androgen receptor (AR) gene (La Spada *et al.*, 1991; Tanaka *et al.*, 1996), and shows somatic mosaicism (Tanaka *et al.*, 1999). An inverse correlation exists between CAG repeat size and age at onset as well as disease severity in SBMA (Doyu *et al.*, 1992; Igarashi *et al.*, 1992; La Spada *et al.*, 1992). SBMA patients develop premature muscular exhaustion, and subsequently slowly progressive muscular weakness, atrophy and fasciculations in bulbar and limb muscles (Kennedy *et al.*, 1968; Sobue *et al.*, 1989; Sperfeld *et al.*, 2002). SBMA patients may also have mild sensory impairment, which usually remains subclinical (Sobue *et al.*, 1989; Li *et al.*, 1995; Mariotti *et al.*, 2000). Besides these symptoms of neuronal degeneration, androgen insensitivity symptoms such as gynaecomastia, testicular atrophy and reduced fertility are common (Arbizu *et al.*, 1983). Elevated serum creatine kinase concentrations, impaired glucose tolerance, hepatic dysfunction and hyperlipidaemia are frequent (Sobue *et al.*, 1989; Li *et al.*, 1995). These findings show that involvement of

© *The Author (2005). Published by Oxford University Press on behalf of the Guarantors of Brain. All rights reserved. For Permissions, please email: journals.permissions@oupjournals.org*

SBMA is not restricted to motor neurons, but extends to several visceral organs.

The cardinal pathological findings of SBMA are motor neuron loss in the spinal cord and brainstem (Sobue *et al.*, 1989) and the presence of the nuclear inclusions (NIs), representing mutant AR, in residual motor neurons in brainstem motor nuclei, in spinal motor neurons (Li *et al.*, 1998*a*) and in certain visceral organs (Li *et al.*, 1998*b*). However, diffuse nuclear accumulation of the mutant protein has been detected in a more widespread distribution than NIs in a transgenic mouse model of SBMA (Katsuno *et al.*, 2002, 2003; Adachi *et al.*, 2003) and in models of other polyQ diseases (Schilling *et al.*, 1999; Yvert *et al.*, 2000; Lin *et al.*, 2001). Such accumulation has been found to be relevant to neuronal dysfunction and eventual symptom appearance. Indeed, in dentatorubral-pallidoluysian atrophy (DRPLA), tissue distribution of diffuse nuclear accumulation of the responsible mutant protein was more widespread and more relevant to the disease severity and symptoms than that of NIs (Yamada *et al.*, 2001*a*, *b*).

Recently we demonstrated in our transgenic mouse model that diffuse nuclear mutant AR accumulation can be prevented by reduction of circulating testosterone with castration or with an anti-androgenic agent such as leuprolerin; in treated animals, motor function and survival rate were dramatically improved (Katsuno *et al.*, 2002, 2003), suggesting that disease manifestation in SBMA is highly testosterone dependent (Lieberman *et al.*, 2002; Walcott and Merry, 2002*a*; Chevalier-Larsen *et al.*, 2004). Indeed, a female carrier of SBMA, even if homozygous, does not express disease phenotypes (Sobue *et al.*, 1993; Schmidt *et al.*, 2002), presumably because circulating testosterone concentrations are low. These observations indicate that nuclear translocation and nuclear accumulation of mutant AR, detected as diffuse nuclear accumulation, is closely linked to the phenotypic expressions and that diffuse nuclear mutant AR accumulation is of major pathogenetic importance in neuronal dysfunction (Katsuno *et al.*, 2002, 2003).

In this study, to understand better the pathophysiology of SBMA, we examined neural and non-neural tissue distributions of mutant AR accumulation in 11 SBMA patients at autopsy, using 1C2, an antibody specific for the expanded polyQ tract, as well as antibodies against AR. First, diffuse nuclear accumulation of mutant AR was far more extensive than that of NIs. Secondly, mutant AR accumulation was also present in cytoplasm, specifically in the Golgi apparatus, with predominance of nuclear or cytoplasmic accumulation being tissue specific. Thirdly, the extent of diffuse nuclear accumulation was closely related to CAG repeat length. Our present results strongly suggested that diffuse nuclear accumulation of mutant AR is of critical pathogenetic importance for motor symptoms as in the SBMA transgenic mouse model, although cytoplasmic accumulation may also contribute to the pathophysiology of SBMA.

Subjects and methods

Patients

Eleven patients with clinicopathologically and genetically confirmed SBMA (age at death, 51–84 years; mean, 66) were examined in this study (Table 1). These patients had been hospitalized and followed-up at Nagoya University Hospital and its affiliated hospitals during the past 25 years. Age at onset ranged between 20 and 75 years, and muscle weakness and bulbar symptoms had progressed for 6–53 years. Elevated serum creatine kinase and glucose was observed in many patients. Causes of death included respiratory failure related to pneumonia in seven patients, lung cancer and colon cancer in one patient each, and tuberculosis and suffocation in one patient each. At autopsy, the brain, spinal cord, dorsal root ganglia, thoracic sympathetic ganglia and various visceral organs were removed and fixed in 10% buffered formalin solution. CAG repeat length in the *AR* gene ranged between 40 and 50. Five other subjects (age 60–74 years, mean 67.3) who died of non-neurological diseases served as controls.

Tissue preparation and immunohistochemistry

We prepared 5 μm thick, formalin-fixed, paraffin-embedded sections of various portions of the cerebrum, brainstem, cerebellum,

Table 1 *Clinical features of 11 SBMA patients*

Patient	Age at death (years)	Onset of limb weakness (years)	CK (normal range)	Glucose (mg/dl)	$(CAG)_n$	Cause of death
1	74	20	455 (57–197)	84*	48	Pneumonia
2	60	27	477 (36–203)	276	50	Pneumonia
3	71	50	995 (53–288)	141	48	Pneumonia
4	60	40	191 (32–197)	134	44	Lung cancer
5	78	25	411 (30–170)	362	42	Pneumonia
6	84	75	75 (<110)	100	40	Tuberculosis, silicosis
7	51	41	712 (30–170)	96*	47	Pneumonia
8	66	41	471 (<120)	163	48	Pneumonia
9	72	39	45 (<25)	101*	43	Colon cancer
10	59	53	301 (8–80)	105*	ND	Suffocation
11	51	27	173 (20–100)	101	ND	Pneumonia

CK = serum creatine kinase; $(CAG)_n$ = number of expanded CAG repeats in the AR allele. $(CAG)_n$ was determined on the DNA from blood samples (patients 1–7) or from stored tissue samples (patients 8 and 9, liver). *Impaired glucose tolerance assessed with 75 g oral glucose tolerance test. ND = not determined.

spinal cord, dorsal root ganglia, sympathetic ganglia, pituitary gland, peripheral nerve, muscle and non-neural visceral organs from SBMA and control subjects. Sections then were deparaffinized and rehydrated through a graded series of alcohol–water solutions. For the mutant AR immunohistochemical study, sections were pre-treated with immersion in 98% formic acid for 5 min and then with microwave oven heating for 10 min in 10 mM citrate buffer at pH 6.0. Sections were blocked with normal serum from the animal species in which each second antibody was raised (1 : 20), and then incubated with a mouse anti-expanded polyQ antibody (Trottier *et al.*, 1995) (1C2; Chemicon, Temecula, CA; 1 : 10 000); a mouse anti-Golgi 58K protein antibody (Sigma, St. Louis, MO; 1 : 100); rabbit polyclonal antibody N-20 (Santa Cruz Biotechnology, Santa Cruz, CA; 1 : 200); rabbit polyclonal antibody PG-21 (Affinity BioReagents, Golden, CO; 1 : 200); rabbit polyclonal antibody H-280 (Santa Cruz; 1 : 200); rabbit polyclonal antibody C-19 (Santa Cruz; 1 : 200); or a mouse monoclonal antibody (Ab-1; Neomarkers, Fremont, CA; ready-to-use) against human AR protein. Then the sections were incubated with biotinylated IgG raised against the species used for each primary antibody (Vector Laboratories, Burlingame, CA). Immune complexes were visualized using streptavidin–horseradish peroxidase (Dako, Glostrup, Denmark) and 3,3′-diaminobenzidine (Dojindo, Kumamoto, Japan) substrate. Sections were counterstained with methyl green or Mayer's haematoxylin. As a negative control, primary antibodies were replaced with normal rabbit or mouse serum. The population of labelled neurons was analysed semi-quantitatively in all 11 SBMA patients, and non-neural visceral organs in nine patients (patients 1–8, and 11) by counting the positive and negative cells for labelling in the region of interest and graded as – to +++.

To assess the co-localization of cytoplasmic mutant AR accumulation and cell organelles, five selected SBMA patients (patients 1, 2, 6, 8 and 10) were analysed by double immunofluorescence staining. The sections were blocked with 5% normal serum and then sequentially incubated at 4°C overnight with any antibody to lysosomal markers, anti-cathepsin B antibody (Ab-3; Oncogene, Cambridge, MA; 1 : 20), anti-cathepsin D antibody (Ab-2; Oncogene; 1 : 20), anti-cathepsin K antibody (N-20; Santa Cruz Biotechnology; 1 : 50), anti-cathepsin L antibody (S-20; Santa Cruz Biotechnology; 1 : 50), antibody to Golgi apparatus, anti-human TGN46 antibody (Serotec, Oxford, UK; 1 : 1000), antibody to endoplasmic reticulum marker, anti-GRP78 antibody (N-20; Santa Cruz; 1 : 200), or antibody to mitochondria, anti-mitochondria antibody (Chemicon; 1 : 50), and 1C2 antibody (Chemicon; 1 : 10 000). Sections were incubated with Alexa 488-conjugated anti-mouse IgG (Molecular Probes, Leiden, The Netherlands; 1 : 1300) and Alexa 568-conjugated IgG raised against the species used for each primary antibody (Molecular Probes; 1 : 1000). For double immunofluorescence staining using anti-human TGN46 antibody, sections were incubated with biotinylated anti-sheep IgG (Vector Laboratories; 1 : 400) for 8 h at 4°C, the sections were incubated with Alexa 568-conjugated streptavidin (Molecular Probes; 1 : 1000) and Alexa 488-conjugated anti-mouse IgG (Molecular Probes; 1 : 1300) for 2 h at 4°C. Sections then were examined and photographed using a confocal laser scanning microscope (MRC 1024; Bio-Rad Laboratories, Hercules, CA).

For electron microscopic immunohistochemistry, buffered formalin-fixed, paraffin-embedded tissue sections were deparaffinized, rehydrated, immunostained with 1C2 antibody (Chemicon, 1 : 10 000), and then incubated with biotinylated anti-mouse IgG (Vector Laboratories; 1 : 1300). Immunoreactivity in tissue sections was visualized using streptavidin–horseradish peroxidase (Dako) and 3,3′-diaminobenzidine substrate (Dojindo), fixed with 2% osmium tetroxide in 0.1 mol/l phosphate buffer at pH 7.4, dehydrated in graded alcohol–water solutions, and embedded in epoxy resin. Ultrathin sections then were cut for observation under an electron microscope (H-7100; Hitachi High-Technologies Corporation, Tokyo, Japan).

Quantification of diffuse nuclear- and NI-positive cell populations

For quantitative assessment, we prepared at least 100 transverse sections each from the cervical, thoracic and lumbar spinal cord for staining with 1C2 antibody as above. The numbers of 1C2-positive and -negative cells in the ventral and dorsal horn on both right and left sides were counted on every 10th section under the light microscope with a computer-assisted image analyser (Luzex FS; Nikon, Tokyo, Japan). For the purposes of counting, a cell was defined by the presence of its nucleus in a given 5 μm thick section. Diffuse nuclear staining and NI-positive neurons were assessed separately. Neurons showing both diffuse nuclear staining and NIs were counted in both categories. The area of the ventral and dorsal horn of each spinal cord section was determined as described previously (Terao *et al.*, 1996; Adachi *et al.*, 2001). Populations of 1C2-positive cells were expressed as percentages of the total neuronal count. For statistical analysis, mean values of these percentages in sections examined from each of the cervical, thoracic and lumbar spinal segments for each patient were obtained.

Statistical analysis

We analysed the data by Pearson's correlation coefficient and Spearman's rank correlation as appropriate using Statview software (version 5; Hulinks, Tokyo, Japan), considering P values <0.05 to be indicative of significance.

Results

Immunohistochemical localization of mutant androgen receptor in the neural tissues

In all 11 patients with SBMA, NIs were visualized clearly with 1C2 (Fig. 1). In addition to NIs, diffusely distributed staining with 1C2 was observed in neuronal nuclei (Fig. 1). Among nuclei with diffuse staining, some showed punctate, granular or web-like patterns, while others showed intense diffuse staining (Fig. 1). In some neurons, NIs and diffuse nuclear staining co-existed (Fig. 1). Moreover, occasional neurons showed granular or punctate 1C2-positive accumulation in the cytoplasm (Fig. 1). As reported previously (Li *et al.*, 1998*a*, *b*), NIs were observed frequently in lower motor neurons, which are known to be affected in this disease. However, we found that neuronal nuclear and cytoplasmic accumulations extended to various regions of the nervous system previously reported to be spared (Li *et al.*, 1998*a*, *b*), including the striatum, caudate nucleus, mammillary body, thalamus, hypothalamus, reticular formation, red nucleus, substantia nigra, locus coerulus, nucleus raphe pontis, pontine nuclei, cuneate nucleus, nucleus ambiguus, gracile nucleus, supraspinal nucleus, cerebellar dentate nucleus, Clarke's

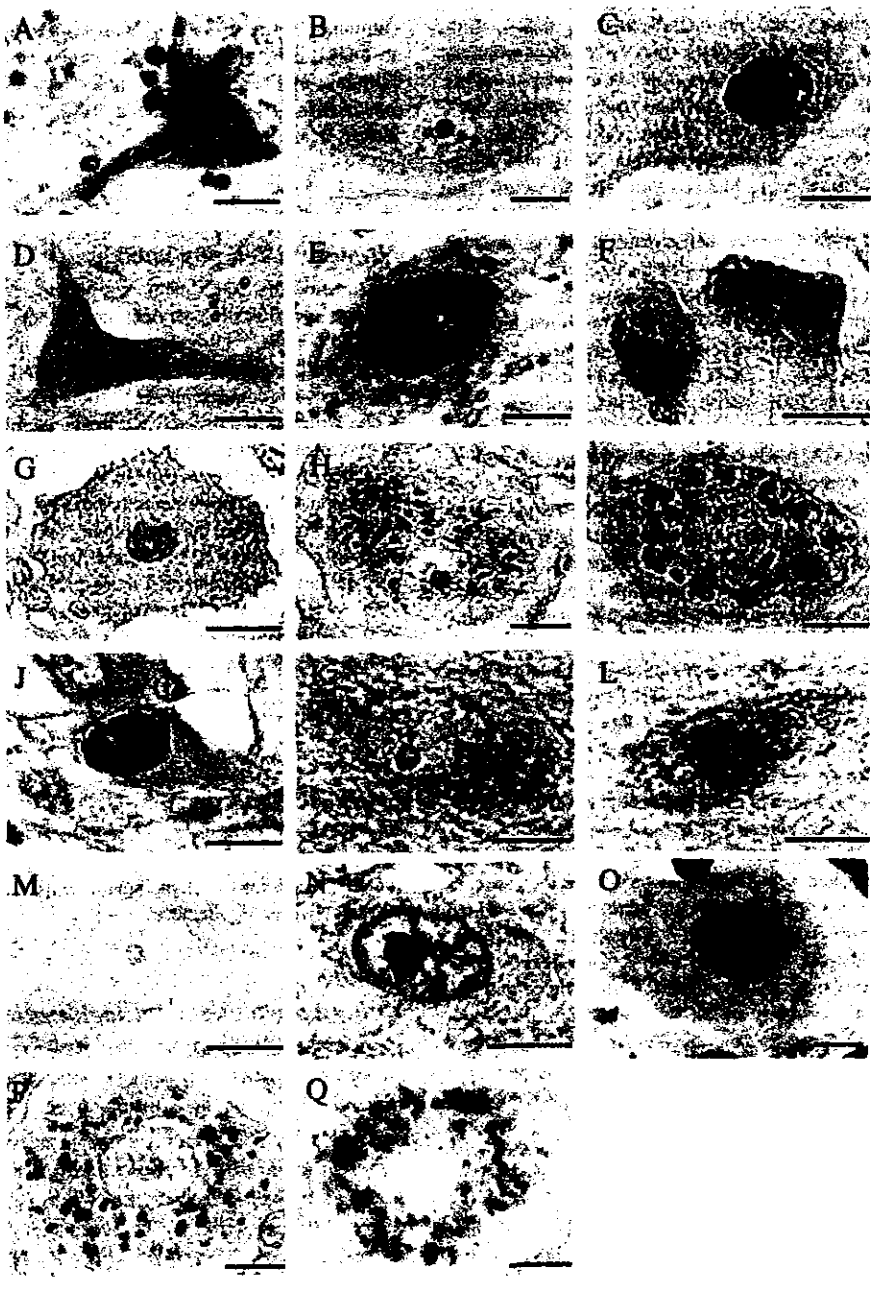

Fig. 1 Immunohistochemical analysis in the neural tissues from SBMA patients and control cases. In the CNS of SBMA patients, intense diffuse nuclear staining is present in neuronal nuclei of various regions using 1C2 antibody (**A**, **E**, **F**, **G**, **J** and **L**). Diffuse immunostaining of mutant androgen receptor (AR) is present in a web-like pattern in nuclei of anterior horn neurons (**A**). Diffuse nuclear staining is also observed in posterior horn neurons (**E**), substantia nigra (**F**), spinal dorsal root ganglia (**G**), paravertebral sympathetic ganglia (**J**) and hypothalamus (**L**). Some nuclei appear packed with mutant AR. Small or large nuclear inclusions are also stained intensely using 1C2 antibody in anterior horn neurons (**B–D**), posterior horn neurons (**E**), the substantia nigra (**F**) and the hypothalamus (**L**). Most of the dark brown pigment seen in the neuronal cytoplasm in the substantia nigra (**F**) is neuromelanin. In addition to nuclear inclusions, occasional neurons exhibit granular structures immunoreactive for 1C2 in the cytoplasm, such as in the anterior horn (**D**) and hypothalamus (**K**). In spinal dorsal root ganglia, small or large cytoplasmic inclusions are frequent (**H** and **I**). There is no immunoreactivity for 1C2 in the spinal anterior horn cell from the control case (**M**). Immunopositive nuclear inclusions and diffuse nuclear staining are also present using H280 antibody in the spinal anterior horn cell (**N**) and spinal dorsal root ganglia (**O**). Spinal dorsal root ganglia neurons exhibit granular structures immunoreactive for anti-Golgi 58K protein antibody in the cytoplasm in SBMA (**P**) and a control case (**Q**). Scale bars = 20 μm for **A**, **D**, **F**, **G**, **M** and **O**; and 10 μm for **B**, **C**, **E**, **H**, **I**, **J**, **K**, **L**, **N**, **P** and **Q**.

nucleus, posterior horn and intermediolateral nucleus of the spinal cord, dorsal root ganglia and sympathetic ganglia (Fig. 1, Table 2). Cytoplasmic inclusions were prominent in the dorsal root ganglia neurons, and some neurons in the mammillary body, hypothalamus and facial motor nucleus and anterior and posterior horns of the spinal cord showed a slight degree of cytoplasmic accumulation (Table 2). We detected both nuclear and cytoplasmic accumulations in some neurons (Fig. 1D). No significant difference in staining pattern was evident between regions previously reported to be affected and unaffected. Diffuse nuclear staining was seen more frequently than NIs in most regions (Table 2). Relative numbers of stained neurons varied between patients, but no staining was detected in cerebral cortex, hippocampus or cerebellar cortex. In contrast to neurons, NIs and diffuse nuclear staining were very rare in glial cells. NIs stained strongly with anti-ubiquitin antibody, while cytoplasmic accumulations did not (data not shown). Anti-human AR antibodies also recognized NIs (Fig. 1N), and occasionally stained diffuse nuclear accumulations (Fig. 1O). However, cytoplasmic accumulations were not seen with anti-AR antibodies.

Table 2 *Immunohistochemical distribution of mutant AR in the neural tissues of patients with SBMA*

Region	Nuclear accumulation		Cytoplasmic accumulation
	Diffuse nuclear accumulation	NI	
Cerebrum			
Cerebral cortex	–	–	–
Striatum	+	+	–
Caudate nucleus	+	+	–
Mammillary body	–	–	+
Thalamic nuclei	+	+	–
Hypothalamus	+ to ++	+	+
Midbrain			
Superior colliculus	–	–	–
Periaqueductal grey	+	+	–
Oculomotor nucleus	–	–	–
Reticular formation of midbrain	+	+	–
Red nucleus	+	+	–
Substantia nigra	+	+	–
Pons			
Locus coerulus	+	+	–
Trigeminal motor nucleus	+ to ++	+	–
Reticular formation of pons	+	+	–
Facial motor nucleus	+ to +++	+	+
Nucleus raphe pontis	+	+	–
Pontine nuclei	+	+	–
Medulla			
Cuneate nucleus	+	+	–
Hypoglossal nucleus	+ to ++	+	–
Nucleus ambiguus	+ to ++	+	–
Gracile nucleus	+	+	–
Supraspinal nucleus	+ to ++	+	–
Accessory nucleus	+	+	–
Cerebellum			
Purkinje cell	–	–	–
Granule cell	–	–	–
Cerebellar dentate nucleus	+	+	–
Spinal cord			
Anterior horn motor neurons	+ to +++	+ to ++	+
Intermediate zone	+	+	–
Clarke's nucleus	+	–	–
Posterior horn neurons	+ to ++	– to +	+
Intermediolateral nucleus	+	+	
Dorsal root ganglia	+	+	++ to +++
Sympathetic ganglia	+	+	–

Frequency of neurons expressing polyglutamine immunoreactivity: –, 0%; +, 0–4%; ++, 4–8%; +++, 8%.

Electron microscopic immunohistochemistry for 1C2 demonstrated granular dense aggregates without a limiting membrane corresponding to NIs and cytoplasmic accumulations, whereas amorphous aggregates corresponded to diffuse nuclear staining in neurons (Fig. 2). No filamentous structures such as those reported in Huntington's disease, DRPLA and Machado–Joseph disease were seen. Neural tissues from five control cases were also examined in the same manner as that for SBMA cases; in these, NIs, diffuse nuclear staining and cytoplasmic accumulations were not seen, indicating that the immunohistochemical procedure with the highly diluted condition of 1C2 applied in this study did not recognize the TATA-binding protein, a transcription factor containing a stretch of polyQ residues (Trottier *et al.*, 1995), as previously demonstrated (Yamada *et al.*, 2001*a*, 2002*a*).

Although we did not quantitatively examine neuronal populations in this study, the motor neurons in the spinal cord and brainstem showed the most conspicuous depletion, as expected. Neurons in the posterior horn of the spinal cord, where diffuse nuclear accumulations and NIs were present in relatively high frequency, also appeared to be depleted to some extent. Quantitative assessment of neuronal cell populations in regions newly showing mutant AR accumulation will be needed.

Co-localization of cytoplasmic organelles with mutant AR

We performed immunofluorescence with double staining using primary antibodies to recognize specifically various cytoplasmic cell organelles together with 1C2 in the dorsal root ganglia, where cytoplasmic mutant AR accumulation was most prominent (Table 2). TGN46 and 1C2 were co-localized (Fig. 3), indicating that mutant AR exists in the Golgi apparatus. Spinal dorsal root ganglia neurons exhibit some granular structures immunoreactive for another Golgi apparatus marker anti-Golgi 58K protein antibody in the cytoplasm (Fig. 1P and Q). Other organelle markers, including antibodies for lysosomes, endoplasmic reticulum and mitochondria, did not show co-localization with 1C2 (Fig. 3), indicating that expanded polyQ sequences were not detected in these organelles.

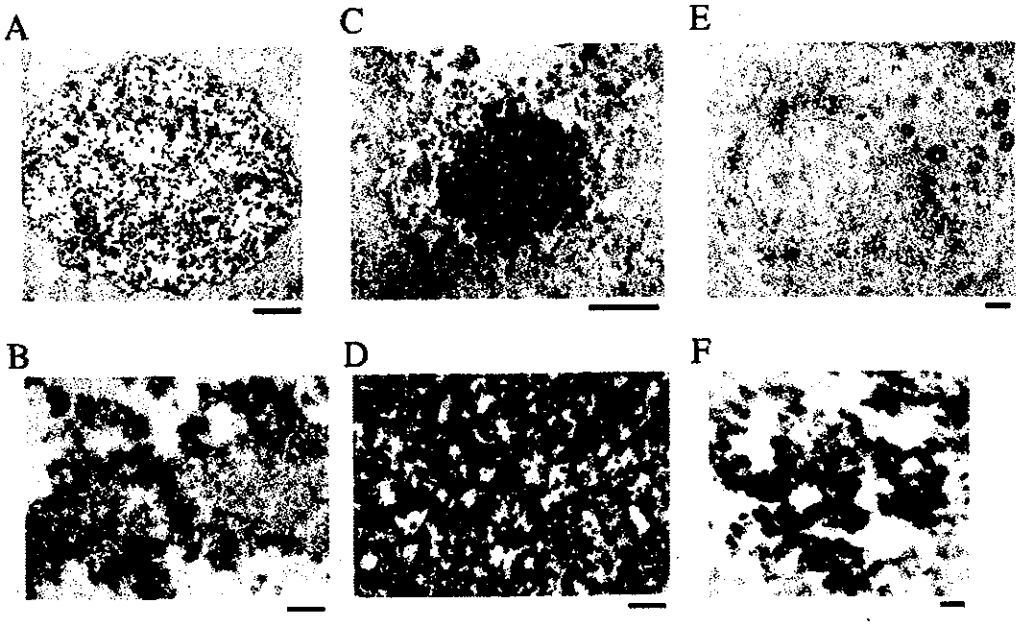

Fig. 2 Electron microscopic immunohistochemical study of nuclear inclusions in motor neurons, and of diffuse nuclear staining and cytoplasmic inclusions in sensory neurons. Electron microscopic immunohistochemistry using 1C2 demonstrated amorphous aggregates corresponding to diffuse nuclear staining in the spinal dorsal root ganglia (**A** and **B**), and granular dense aggregates without fibrous configurations corresponding to nuclear and cytoplasmic inclusions in the spinal anterior neuron (**C** and **D**) and spinal dorsal root ganglia (**E** and **F**). Scale bars = 2 μm for **A**, **C** and **E**; and 200 nm for **B**, **D** and **F**.

Correlation of diffuse nuclear accumulation and NIs with degree of CAG repeat expansion

We examined the correlation of diffuse nuclear accumulation and NIs with the degree of CAG repeat expansion in anterior and posterior horn spinal cord neurons. Averaged frequencies of diffuse nuclear accumulations and NIs in cervical, thoracic and lumbar spinal segments were evaluated for correlation with numbers of CAG repeats in the *AR* gene. The frequency of diffuse nuclear accumulation in anterior and posterior horn neurons correlated well with the degree of CAG repeat expansion (Fig. 4; $r = 0.78$, $P < 0.05$ and $r = 0.69$, $P < 0.05$, respectively). However, the frequency of NIs in motor neurons and posterior horn neurons did not show a significant correlation with number of CAG repeats (Fig. 4; $r = 0.05$, P = NS and $r = -0.14$, P = NS, respectively). These observations strongly suggest that diffuse nuclear accumulation of the mutant AR protein is more important pathogenetically than NIs.

Immunohistochemical localization of mutant AR in non-neural tissues

As in neural tissues, diffuse nuclear accumulations, NIs or cytoplasmic accumulations of mutant AR were observed in certain visceral organs and skin (Fig. 5, Table 3). Diffuse nuclear accumulations and NIs were detected in the liver, proximal tubules of the kidney, testis, prostate gland, and scrotal and other skin (Fig. 5, Table 3). Cytoplasmic accumulations were detected in the liver, pancreatic islets of Langerhans, testis and prostate gland (Fig. 5, Table 3). Nuclear labelling and cytoplasmic accumulation both were absent in the pituitary gland, heart, lung, intestine, spleen, thyroid, adrenal gland and skeletal muscles. Pancreatic islet cells showed exclusively cytoplasmic accumulations without detectable nuclear accumulations, suggesting that the impaired glucose tolerance frequently observed in our patients (Table 1) could be attributed to cytoplasmic mutant AR accumulation. Ubiquitin staining detected only NIs and, as observed in neural tissues, anti-human AR antibodies occasionally showed diffuse nuclear accumulation without cytoplasmic staining (Fig. 5J). The five control cases did not show any 1C2 immunoreactivity in viscera or skin.

Discussion

The present study clearly demonstrated that diffuse nuclear accumulation of mutant AR, detected by the antibody 1C2 which specifically recognizes the expanded polyQ tract, occurred more frequently than NIs in neural and non-neural tissues in SBMA patients. In neural tissues, diffuse nuclear mutant AR accumulation occurred in the basal ganglia, thalamus, hypothalamus, various midbrain, pontine and medullary nuclei, posterior horn, intermediolateral and Clarke's nuclei of the spinal cord and in sensory and sympathetic ganglion neurons, as well as brainstem and spinal cord motor neurons. NIs detected by 1C2 were similar

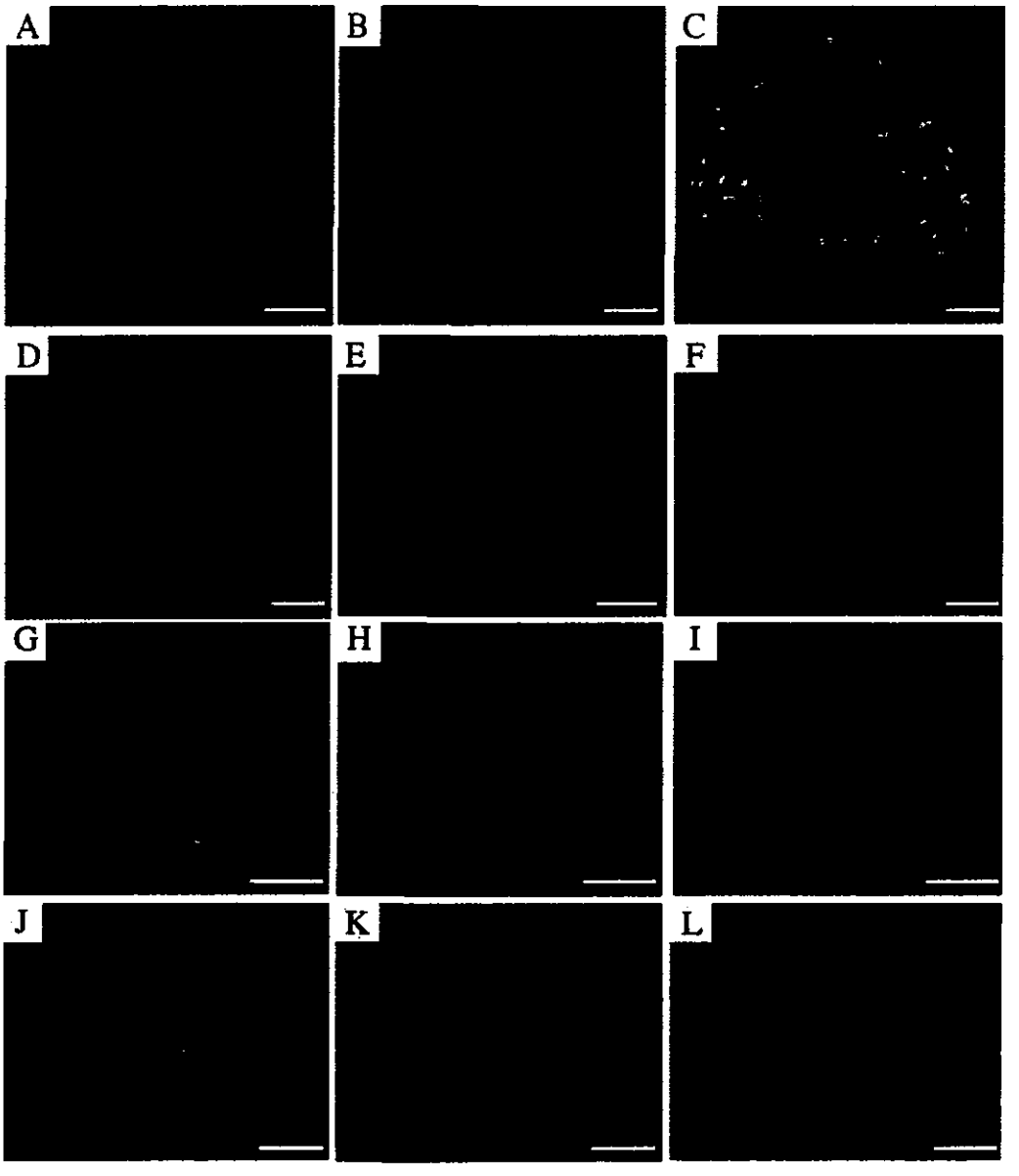

Fig. 3 Co-localization of organelles with mutant AR accumulation. Double immunofluorescence staining with antibodies against TGN46 and expanded polyQ reveals that TGN46 and mutant androgen receptor (AR) are co-localized, as shown for (**A**) expanded polyQ (green), (**B**) TGN46 (red) and (**C**) superimposition of the two signals (yellow) in neurons of the spinal dorsal root ganglia in SBMA, suggesting that mutant AR exists in the Golgi apparatus. Cytoplasmic co-localization of cathepsin B (**E**), GRP78 (**H**) and mitochondria (**K**) with mutant AR (**D**, **G** and **J**) is not observed in dorsal root ganglia (shown in **F**, **I** and **L**), suggesting that the endoplasmic reticulum, lysosomes and mitochondria are unassociated with mutant AR. Scale bars = 10 μm for **A–L**.

in distribution to diffuse nuclear accumulation, but the frequency of NIs in each tissue was far less than for diffuse nuclear accumulation. We previously demonstrated that diffuse nuclear mutant AR protein accumulation was more extensive than NIs in male SBMA transgenic mice (Katsuno *et al.*, 2002, 2003). Furthermore, expression and severity of motor dysfunction, and abatement of abnormalities when the mice were castrated or given leuprolerin, paralleled the extent of diffuse nuclear mutant AR accumulation rather than that of NIs (Katsuno *et al.*, 2002, 2003). Accordingly, neuronal dysfunction appeared to be closely related to diffuse nuclear mutant AR accumulation. The key observation in the present study was a significant close correlation between frequency of diffuse nuclear mutant AR accumulation and length of CAG repeat expansion, while a similar correlation was not observed between frequency of NIs and CAG repeats. Diffuse nuclear

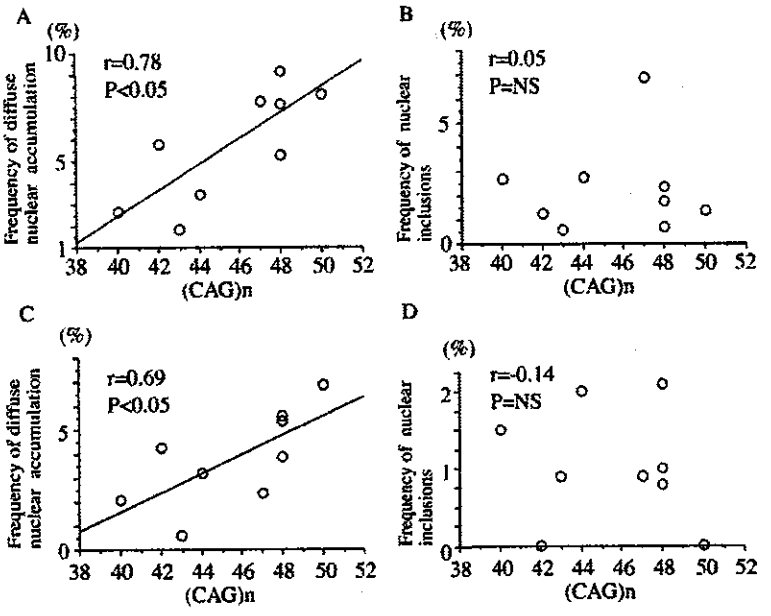

Fig. 4 The relationship of the number of CAG repeats to the frequency of diffuse nuclear accumulation and nuclear inclusions. Diffuse nuclear staining correlates significantly with the number of CAG repeats in anterior horn neurons (**A**) and posterior horn neurons (**C**). On the other hand, nuclear inclusions do not correlate significantly with the number of CAG repeats in the anterior horn neurons (**B**) or posterior horn neurons (**D**).

mutant protein accumulation also has been demonstrated in the neural tissues affected by DRPLA (Yamada *et al.*, 2001*a*, 2002*a*), Huntington's disease (Sapp *et al.*, 1997) and Machado–Joseph disease (Yamada *et al.*, 2001*b*) as well as corresponding transgenic mouse models (Schilling *et al.*, 1999; Yvert *et al.*, 2000; Lin *et al.*, 2001); and, here too, diffuse nuclear mutant protein accumulation was more widespread and extensive than NIs in DRPLA patients. These observations are in good agreement with our present observation in SBMA patients; together, they suggest that diffuse nuclear accumulation of mutant proteins with an expanded polyQ tract is an early event prior to NI formation that is closely related to manifestation of neuronal dysfunction (Yamada *et al.*, 2001*a*; Garden *et al.*, 2002; Katsuno *et al.*, 2002, 2003; Watase *et al.*, 2002; Yoo *et al.*, 2003). However, the molecular pathogenetic process by which diffuse nuclear mutant AR accumulation induces neuronal dysfunction still is unclear. Although considerable controversy recently surrounds the importance of NIs in the pathophysiology in polyQ diseases (Simeoni *et al.*, 2000; Walcott and Merry, 2002*b*; Bates, 2003; Michalik and Van Broeckhoven, 2003; Ross *et al.*, 2003), our data showed that diffuse mutant AR accumulation in nuclei could have potent cytotoxic effects inducing neuronal dysfunction through an active epitope of the expanded polyQ tract.

Anti-AR antibodies showed the ability to detect NIs, and some of them (H280, N-20 and Ab-1) occasionally stained diffuse nuclear accumulations. Diffuse nuclear accumulation had the appearance of amorphous aggregates of mutant AR as observed by electron microscopic immunohistochemistry using 1C2 (Fig. 2) (Katsuno *et al.*, 2002). These observations suggest that the polyQ tract epitope can be detected by 1C2, while other AR protein epitopes may be protected by structural features of the aggregate state of the mutant AR. This view is supported by observations made by small-angle X-ray scattering and infrared spectroscopy carried out with myoglobin protein containing an inserted highly expanded polyQ tract, localizing the polyQ tract to the surface of aggregates, while other epitopes were sequestered within aggregates (Tanaka *et al.*, 2001, 2003). These observations suggest that 1C2 can detect the amorphous aggregate state of mutant AR protein, making 1C2 a more sensitive histological and pathophysiological marker than anti-AR protein antibodies. On the other hand, cytoplasmic accumulations were not seen with anti-AR antibodies. This cytoplasmic mutant AR was not ubiquitinated, in contrast to nuclear accumulated mutant AR, particularly the heavily ubiquitinated NIs, suggesting that protein modification varies between the nucleus and cytoplasm. Different protein modification might mask other AR protein epitopes directly or through structural alterations of the aggregate state of the mutant AR in the cytoplasm.

Another important observation in our study was the occurrence of cytoplasmic mutant AR accumulation in neural and non-neural tissues. In neural tissues, cytoplasmic accumulation was restricted to certain neuronal populations such as dorsal root ganglia neurons, mammillary body, hypothalamus, facial motor nucleus, and anterior and posterior horn neurons. In non-neural tissues, cytoplasmic accumulation also occurred in certain organs. Cytoplasmic mutant AR accumulation co-localized with a Golgi apparatus marker.

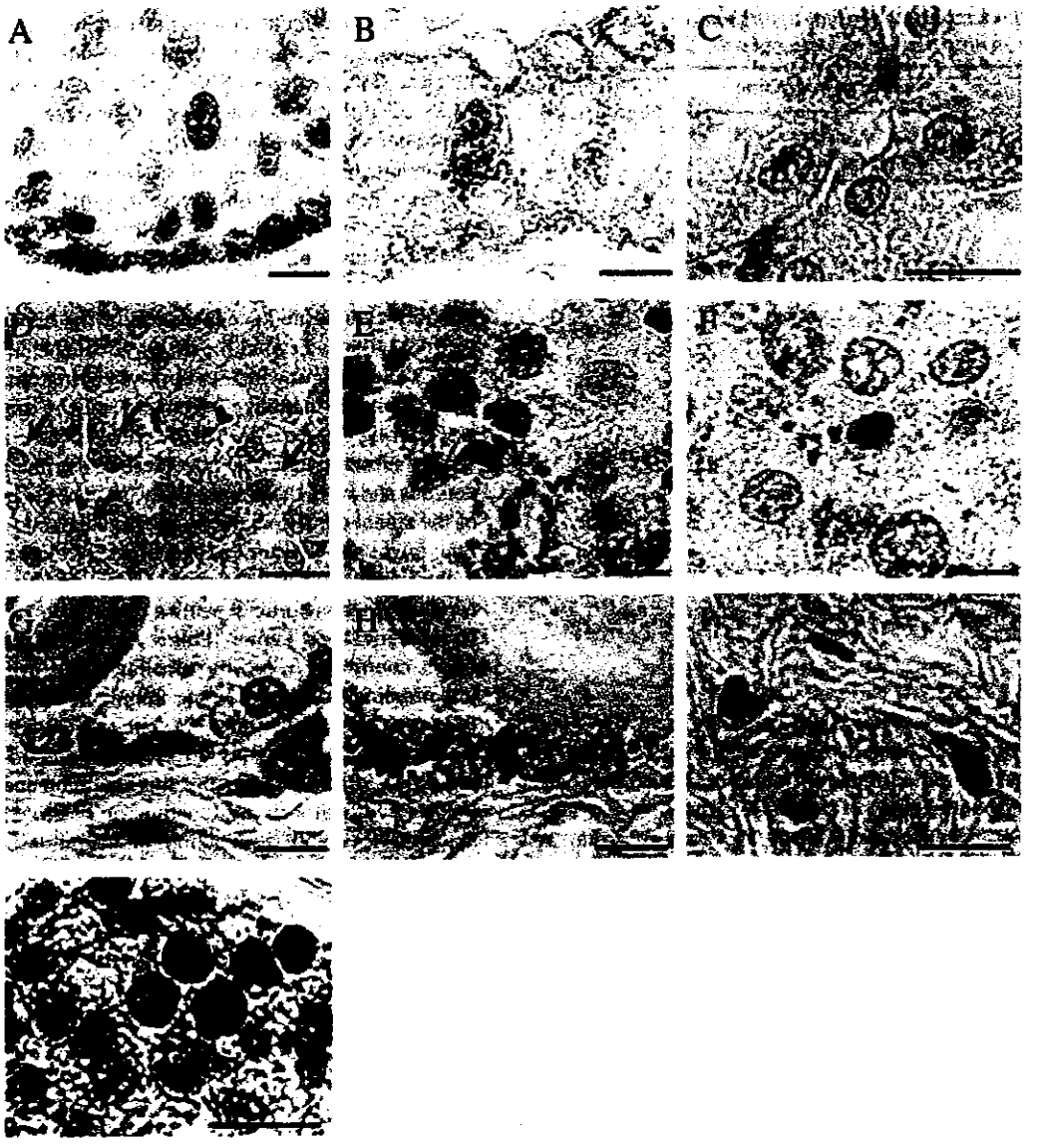

Fig. 5. Immunohistochemical study of the non-neural tissues in SBMA patients using 1C2 antibody. In the non-neural tissues, diffuse nuclear staining and nuclear inclusions are detectable in scrotal skin (**A**), other skin (**B**), proximal tubules of the kidney (**C**), hepatocytes (**D**), Sertoli cells of the testis (**E**), and glandular epithelium (**G**) and fibroblasts of the interstitial connective tissue (**I**) of the prostate gland. Moreover, cytoplasmic inclusions can be detected in hepatocytes (**D**), spermatocytes in the testis (**E**), pancreatic islets of Langerhans (**F**) and glandular epithelium of the prostate gland (**H**). Diffuse nuclear staining is also present using H280 antibody in Sertoli cells of the testis (**J**). Scale bars = 10 μm for **A–C** and **E–I**; and 20 μm for **D** and **J**.

Co-localization of a polyQ-expanded mutant protein with the Golgi apparatus has also been reported for ataxin-2 (Huynh *et al.*, 2003), although the significance of this localization remains unclear. Expression of polyQ-expanded mutant ataxin-2 disrupted the normal morphology of the Golgi complex and increased cell death (Huynh *et al.*, 2003). On the other hand, the lysosomal occurrence of other mutant proteins with an expanded polyQ tract has been reported in DRPLA (Yamada *et al.*, 2002*b*) and Huntington's disease (Sapp *et al.*, 1997). The lysosomal localization of polyQ-expanded mutant proteins suggests a lysosomal autophagic degradation process acting independently of the ubiquitin–proteasome pathway in the polyQ diseases (Sapp *et al.*, 1997). Additionally, the reason why neural tissues develop more nuclear than cytoplasmic accumulation while most involved visceral organs show equal or predominantly cytoplasmic accumulation is unknown. Differences in the predominant degradation pathway dealing with the mutant AR could influence the intracellular site of accumulation and eventual cell toxicity. One important question is whether cytoplasmic mutant AR

Table 3 *Immunohistochemical distribution of mutant AR in the non-neural tissues of patients with SBMA*

Region	Nuclear accumulation		Cytoplasmic accumulation
	Diffuse nuclear accumulation	NI	
Pituitary gland	–	–	–
Heart	–	–	–
Lung	–	–	–
Liver	+	+	+
Kidney	+ to ++	+	–
Pancreas	–	–	+ to ++
Intestine	–	–	–
Spleen	–	–	–
Thyroid	–	–	–
Adrenal gland	–	–	–
Testis	+ to ++	+	+ to ++
Prostate gland	+ to +++	+ to ++	+ to +++
Skeletal muscle	–	–	–
Scrotal skin	+ to +++	+	–
Skin	+ to ++	+	–

Frequency of cells expressing polyglutamine immunoreactivity: –, 0%; +, 0–3%; ++, 3–6%; +++, 6%.

accumulation exerts cytotoxicity in neural and non-neural tissues. Cytoplasmic mutant AR accumulation (Taylor *et al.*, 2003) as well as other mutant protein accumulations (Kegel *et al.*, 2000; Ravikumar *et al.*, 2002; Huynh *et al.*, 2003) involving an expanded polyQ tract in Golgi apparatus and lysosomes indeed has been found to induce cytotoxicity. Accumulation of mutant protein with expanded polyQ in the Golgi apparatus or lysosomes increases death of cultured cells through activation of apoptosis-related effectors such as caspase-3 (Ishisaka *et al.*, 1998; Kegel *et al.*, 2000; Huynh *et al.*, 2003). One should note that histologically or immunohistochemically evident mutant protein accumulation is not necessarily cytotoxic, while microaggregates at the molecular level that are histologically undetectable can also exert cytotoxicity. Indeed, excessive accumulation of mutant AR in aggresomes was found to protect cells from a cytotoxic form of mutant AR (Taylor *et al.*, 2003). However, our present study strongly suggests that these cytoplasmic mutant AR accumulations may be related to mutant AR-mediated cytotoxicity and eventual symptom manifestation. For instance, the pancreas showed only cytoplasmic mutant AR accumulation without obvious nuclear accumulation. Elevated serum glucose and impaired glucose tolerance were present in most of our patients, suggesting islet cell dysfunction in the pancreas. The frequency of cytoplasmic accumulations of mutant AR in pancreatic islet cells did not show a significant correlation with fasting blood glucose levels in the examined SBMA patients (data not shown), while certain symptoms and signs of SBMA apparently can be induced by cytoplasmic accumulation of mutant AR protein. Although further study of the significance of cytoplasmic mutant AR accumulation is needed, nuclear accumulation of the mutant AR protein appears to cause motor neuron dysfunction while cytoplasmic accumulation may underlie some visceral and possibly some neuronal dysfunction in SBMA. The pathological process is likely to differ between tissues, being more prominent in motor neuron nuclei, but mainly cytoplasmic in certain neuronal populations and visceral organs. We also need to clarify further which degradation process affecting mutant AR is most active in a given tissue, e.g. lysosomal in certain viscera versus via ubiquitination pathway in most neural tissues.

An important question here is why diffuse nuclear and possibly cytoplasmic accumulation of the mutant AR in the neuronal tissues beyond the major affected spinal and brainstem motor neurons has no apparent symptomatic involvement. First, the causative lesions for sensory impairment and essential-type tremor in SBMA patients have not yet been clearly substantiated. The novel lesion distribution of SBMA neurons shown in the present study, such as the posterior horn of the spinal cord, dorsal root ganglia, thalamus and cerebellum, might provide some explanations for these clinicopathological problems that have not been resolved. Since the cerebellothalamocortical pathway seems to be responsible for essential-type tremor (Pinto *et al.*, 2003), these lesions might contribute to mostly subclinical but definite sensory impairment and essential-type tremor in SBMA. Secondly, the occurrence of neuronal nuclear and cytoplasmic abnormalities in both clinically affected and non-affected neural regions in SBMA suggests that this alteration does not always induce neuronal cell dysfunction or death. The selective neuronal loss and dysfunction in neural lesions that are characteristic of SBMA might depend on additional factors that are specific to neurons in these systems. Recent studies have demonstrated that CREB-binding protein (CBP) is sequestered in AR-positive NIs, resulting in a decrease in CBP-dependent transcription (McCampbell *et al.*, 2000), and further histone acetylation is reduced in affected cells (McCampbell *et al.*, 2001; Steffan *et al.*, 2001; Minamiyama *et al.*, 2004). These reports suggest that CBP-dependent transcriptional dysregulations may cause symptomatic neuronal dysfunction. Since CBP-dependent transcriptional control differs among neurons, this difference may show the lack of their symptomatic involvement in certain polyQ-containing neurons. Alternatively, the population of neurons with nuclear accumulation of mutant AR in the regions beyond the commonly affected lesions may not be simply enough to manifest the responsible symptoms. A precise neuronal cell count assay combined with assessment of nuclear mutant AR accumulation will be needed to clarify these clinicopathological problems.

Clearly, motor neuron impairment with nuclear accumulation of mutant AR is the major problem in SBMA. Thus, for a therapeutic strategy against motor neuron dysfunction in SBMA, nuclear accumulation of mutant AR should be the main target, as we demonstrated in transgenic mice treated with leuprolerin. Cytoplasmic accumulation of mutant AR, on the other hand, should be considered a therapeutic target with respect to certain symptoms in SBMA patients.

Acknowledgements

We wish to thank Dr Yasushi Iwasaki and Mrs Sugiko Yokoi for technical assistance. This work was supported by a Center of Excellence (COE) grant from the Ministry of Education, Culture, Sports, Science, and Technology of Japan, and grants from the Ministry of Health, Labor, and Welfare of Japan.

References

Adachi H, Kume A, Li M, Nakagomi Y, Niwa H, Do J, et al. Transgenic mice with an expanded CAG repeat controlled by the human AR promoter show polyglutamine nuclear inclusions and neuronal dysfunction without neuronal cell death. Hum Mol Genet 2001; 10: 1039–48.

Adachi H, Katsuno M, Minamiyama M, Sang C, Pagoulatos G, Angelidis C, et al. Heat shock protein 70 chaperone overexpression ameliorates phenotypes of the spinal and bulbar muscular atrophy transgenic mouse model by reducing nuclear-localized mutant androgen receptor protein. J Neurosci 2003; 23: 2203–11.

Arbizu T, Santamaria J, Gomez JM, Quilez A, Serra JP. A family with adult spinal and bulbar muscular atrophy, X-linked inheritance and associated testicular failure. J Neurol Sci 1983; 59: 371–82.

Bates G. Huntingtin aggregation and toxicity in Huntington's disease. Lancet 2003; 361: 1642–4.

Chevalier-Larsen ES, O'Brien CJ, Wang H, Jenkins SC, Holder L, Lieberman AP, et al. Castration restores function and neurofilament alterations of aged symptomatic males in a transgenic mouse model of spinal and bulbar muscular atrophy. J Neurosci 2004; 24: 4778–86.

Doyu M, Sobue G, Mukai E, Kachi T, Yasuda T, Mitsuma T, et al. Severity of X-linked recessive bulbospinal neuronopathy correlates with size of the tandem CAG repeat in androgen receptor gene. Ann Neurol 1992; 32: 707–10.

Garden GA, Libby RT, Fu YH, Kinoshita Y, Huang J, Possin DE, et al. Polyglutamine-expanded ataxin-7 promotes non-cell-autonomous Purkinje cell degeneration and displays proteolytic cleavage in ataxic transgenic mice. J Neurosci 2002; 22: 4897–905.

Huynh DP, Yang HT, Vakharia H, Nguyen D, Pulst SM. Expansion of the polyQ repeat in ataxin-2 alters its Golgi localization, disrupts the Golgi complex and causes cell death. Hum Mol Genet 2003; 12: 1485–96.

Igarashi S, Tanno Y, Onodera O, Yamazaki M, Sato S, Ishikawa A, et al. Strong correlation between the number of CAG repeats in androgen receptor genes and the clinical onset of features of spinal and bulbar muscular atrophy. Neurology 1992; 42: 2300–2.

Ishisaka R, Utsumi T, Yabuki M, Kanno T, Furuno T, Inoue M, et al. Activation of caspase-3-like protease by digitonin-treated lysosomes. FEBS Lett 1998; 435: 233–6.

Katsuno M, Adachi H, Kume A, Li M, Nakagomi Y, Niwa H, et al. Testosterone reduction prevents phenotypic expression in a transgenic mouse model of spinal and bulbar muscular atrophy. Neuron 2002; 35: 843–54.

Katsuno M, Adachi H, Doyu M, Minamiyama M, Sang C, Kobayashi Y, et al. Leuprorelin rescues polyglutamine-dependent phenotypes in a transgenic mouse model of spinal and bulbar muscular atrophy. Nat Med 2003; 9: 768–73.

Kegel KB, Kim M, Sapp E, McIntyre C, Castano JG, Aronin N, et al. Huntingtin expression stimulates endosomal-lysosomal activity, endosome tubulation and autophagy. J Neurosci 2000; 20: 7268–78.

Kennedy WR, Alter M, Sung JH. Progressive proximal spinal and bulbar muscular atrophy of late onset. A sex-linked recessive trait. Neurology 1968; 18: 671–80.

La Spada AR, Wilson EM, Lubahn DB, Harding AE, Fischbeck KH. Androgen receptor gene mutations in X-linked spinal and bulbar muscular atrophy. Nature 1991; 352: 77–9.

La Spada AR, Roling DB, Harding AE, Warner CL, Spiegel R, Hausmanowa-Petrusewicz I, et al. Meiotic stability and genotype–phenotype correlation of the trinucleotide repeat in X-linked spinal and bulbar muscular atrophy. Nat Genet 1992; 2: 301–4.

Li M, Sobue G, Doyu M, Mukai E, Hashizume Y, Mitsuma T. Primary sensory neurons in X-linked recessive bulbospinal neuropathy: histopathology and androgen receptor gene expression. Muscle Nerve 1995; 18: 301–8.

Li M, Miwa S, Kobayashi Y, Merry DE, Yamamoto M, Tanaka F, et al. Nuclear inclusions of the androgen receptor protein in spinal and bulbar muscular atrophy. Ann Neurol 1998a; 44: 249–54.

Li M, Nakagomi Y, Kobayashi Y, Merry DE, Tanaka F, Doyu M, et al. Nonneural nuclear inclusions of androgen receptor protein in spinal and bulbar muscular atrophy. Am J Pathol 1998b; 153: 695–701.

Lieberman AP, Harmison G, Strand AD, Olson JM, Fischbeck KH. Altered transcriptional regulation in cells expressing the expanded polyglutamine androgen receptor. Hum Mol Genet 2002; 11: 1967–76.

Lin CH, Tallaksen-Greene S, Chien WM, Cearley JA, Jackson WS, Crouse AB, et al. Neurological abnormalities in a knock-in mouse model of Huntington's disease. Hum Mol Genet 2001; 10: 137–44.

Mariotti C, Castellotti B, Pareyson D, Testa D, Eoli M, Antozzi C, et al. Phenotypic manifestations associated with CAG-repeat expansion in the androgen receptor gene in male patients and heterozygous females: a clinical and molecular study of 30 families. Neuromuscul Disord 2000; 10: 391–7.

McCampbell A, Taylor JP, Taye AA, Robitschek J, Li M, Walcott J, et al. CREB-binding protein sequestration by expanded polyglutamine. Hum Mol Genet 2000; 9: 2197–202.

McCampbell A, Taye AA, Whitty L, Penney E, Steffan JS, Fischbeck KH. Histone deacetylase inhibitors reduce polyglutamine toxicity. Proc Natl Acad Sci USA 2001; 98: 15179–84.

Michalik A, Van Broeckhoven C. Pathogenesis of polyglutamine disorders: aggregation revisited. Hum Mol Genet 2003; 12: R173–86.

Minamiyama M, Katsuno M, Adachi H, Waza M, Sang C, Kobayashi Y, et al. Sodium butyrate ameliorates phenotypic expression in a transgenic mouse model of spinal and bulbar muscular atrophy. Hum Mol Genet 2004; 13: 1183–92.

Pinto AD, Lang AE, Chen R. The cerebellothalamocortical pathway in essential tremor. Neurology 2003; 60: 1985–7.

Ravikumar B, Duden R, Rubinsztein DC. Aggregate-prone proteins with polyglutamine and polyalanine expansions are degraded by autophagy. Hum Mol Genet 2002; 11: 1107–17.

Ross CA. Polyglutamine pathogenesis: emergence of unifying mechanisms for Huntington's disease and related disorders. Neuron 2002; 35: 819–22.

Ross CA, Poirier MA, Wanker EE, Amzel M. Polyglutamine fibrillogenesis: the pathway unfolds. Proc Natl Acad Sci USA 2003; 100: 1–3.

Sapp E, Schwarz C, Chase K, Bhide PG, Young AB, Penney J, et al. Huntingtin localization in brains of normal and Huntington's disease patients. Ann Neurol 1997; 42: 604–12.

Schilling G, Wood JD, Duan K, Slunt HH, Gonzales V, Yamada M, et al. Nuclear accumulation of truncated atrophin-1 fragments in a transgenic mouse model of DRPLA. Neuron 1999; 24: 275–86.

Schmidt BJ, Greenberg CR, Allingham-Hawkins DJ, Spriggs EL. Expression of X-linked bulbospinal muscular atrophy (Kennedy disease) in two homozygous women. Neurology 2002; 59: 770–2.

Simeoni S, Mancini MA, Stenoien DL, Marcelli M, Weigel NL, Zanisi M, et al. Motoneuronal cell death is not correlated with aggregate formation of androgen receptors containing an elongated polyglutamine tract. Hum Mol Genet 2000; 9: 133–44.

Sobue G, Hashizume Y, Mukai E, Hirayama M, Mitsuma T, Takahashi A. X-linked recessive bulbospinal neuronopathy. A clinicopathological study. Brain 1989; 12: 209–32.

Sobue G, Doyu M, Kachi T, Yasuda T, Mukai E, Kumagai T, et al. Subclinical phenotypic expressions in heterozygous females of X-linked recessive bulbospinal neuronopathy. J Neurol Sci 1993; 117: 74–8.

Sperfeld AD, Karitzky J, Brummer D, Schreiber H, Haussler J, Ludolph AC, et al. X-linked bulbospinal neuronopathy: Kennedy disease. Arch Neurol 2002; 59: 1921–6.

Steffan JS, Bodai L, Pallos J, Poelman M, McCampbell A, Apostol BL, et al. Histone deacetylase inhibitors arrest polyglutamine-dependent neurodegeneration in Drosophila. Nature 2001; 413: 739–43.

Tanaka F, Doyu M, Ito Y, Matsumoto M, Mitsuma T, Abe K, et al. Founder effect in spinal and bulbar muscular atrophy (SBMA). Hum Mol Genet 1996; 5: 1253–7.

Tanaka F, Reeves MF, Ito Y, Matsumoto M, Li M, Miwa S, et al. Tissue-specific somatic mosaicism in spinal and bulbar muscular atrophy (SBMA) is dependent on CAG repeat length and androgen receptor gene expression level. Am J Hum Genet 1999; 65: 966–73.

Tanaka M, Morishima I, Akagi T, Hashikawa T, Nukina N. Intra- and intermolecular beta-plated sheet formation in glutamine-repeat inserted myoglobin as a model for polyglutamine diseases. J Biol Chem 2001; 276: 45470–5.

Tanaka M, Machida Y, Nishikawa Y, Akagi T, Hashikawa T, Fujisawa T, et al. Expansion of polyglutamine induces the formation of quasi-aggregate in the early stage of protein fibrillization. J Biol Chem 2003; 278: 34717–24.

Taylor JP, Tanaka F, Robitschek J, Sandoval CM, Taye A, Markovic-Plese S, et al. Aggresomes protect cells by enhancing the degradation of toxic polyglutamine-containing protein. Hum Mol Genet 2003; 12: 749–57.

Terao S, Sobue G, Hashizume Y, Li M, Inagaki T, Mitsuma T. Age-related changes in human spinal ventral horn cells with special reference to the loss of small neurons in the intermediate zone: a quantitative analysis. Acta Neuropathol (Berl) 1996; 92: 109–14.

Trottier Y, Lutz Y, Stevanin G, Imbert G, Devys D, Cancel G, et al. Polyglutamine expansion as a pathological epitope in Huntingtin's disease and four dominant cerebellar ataxias. Nature 1995; 378: 403–6.

Walcott JL, Merry DE. Ligand promotes intranuclear inclusions in a novel cell model of spinal and bulbar muscular atrophy. J Biol Chem 2002a; 277: 50855–9.

Walcott JL, Merry DE. Trinucleotide repeat disease. The androgen receptor in spinal and bulbar muscular atrophy. Vitam Horm 2002b; 65: 127–47.

Watase K, Weeber EJ, Xu B, Antalffy B, Yuva-Paylor L, Hashimoto K, et al. A long CAG repeat in the mouse Sca1 locus replicates SCA1 features and reveals the impact of protein solubility on selective neurodegeneration. Neuron 2002; 34: 905–19.

Yamada M, Wood JD, Shimohata T, Hayashi S, Tsuji S, Ross CA, et al. Widespread occurrence of intranuclear atrophin-1 accumulation in the central nervous system neurons of patients with dentatorubral-pallidoluysian atrophy. Ann Neurol 2001a; 49: 14–23.

Yamada M, Hayashi S, Tsuji S, Takahashi H. Involvement of the cerebral cortex and autonomic ganglia in Machado–Joseph disease. Acta Neuropathol (Berl) 2001b; 101: 140–4.

Yamada M, Sato T, Tsuji S, Takahashi H. Oligodendrocytic polyglutamine pathology in dentatorubral-pallidoluysian atrophy. Ann Neurol 2002a; 52: 670–4.

Yamada M, Tsuji S, Takahashi H. Involvement of lysosomes in the pathogenesis of CAG repeat diseases. Ann Neurol 2002b; 52: 498–503.

Yoo SY, Pennesi ME, Weeber EJ, Xu B, Atkinson R, Chen S, et al. SCA7 knock in mice model human SCA7 and reveal gradual accumulation of mutant ataxin-7 in neurons and abnormalities in short-term plasticity. Neuron 2003; 37: 383–401.

Yvert G, Lindenberg KS, Picaud S, Landwehrmeyer GB, Sahel JA, Mandel JL. Expanded polyglutamines induce neurodegeneration and trans-neuronal alterations in cerebellum and retina of SCA7 transgenic mice. Hum Mol Genet 2000; 9: 2491–506.

Gene Expression Profile of Spinal Motor Neurons in Sporadic Amyotrophic Lateral Sclerosis

Yue-Mei Jiang, PhD,[1] Masahiko Yamamoto, MD,[1] Yasushi Kobayashi, MD,[1] Tsuyoshi Yoshihara, PhD,[1] Yideng Liang, PhD,[1] Shinichi Terao, MD,[2] Hideyuki Takeuchi, MD,[1] Shinsuke Ishigaki, MD,[1] Masahisa Katsuno, MD,[1] Hiroaki Adachi, MD,[1] Jun-ichi Niwa, MD,[1] Fumiaki Tanaka, MD,[1] Manabu Doyu, MD,[1] Mari Yoshida, MD,[3] Yoshio Hashizume, MD,[3] and Gen Sobue, MD[1]

The causative pathomechanism of sporadic amyotrophic lateral sclerosis (ALS) is not clearly understood. Using microarray technology combined with laser-captured microdissection, gene expression profiles of degenerating spinal motor neurons isolated from autopsied patients with sporadic ALS were examined. Gene expression was quantitatively assessed by real-time reverse transcription polymerase chain reaction and in situ hybridization. Spinal motor neurons showed a distinct gene expression profile from the whole spinal ventral horn. Three percent of genes examined were downregulated, and 1% were upregulated in motor neurons. Downregulated genes included those associated with cytoskeleton/axonal transport, transcription, and cell surface antigens/receptors, such as dynactin, microtubule-associated proteins, and early growth response 3 (EGR3). In contrast, cell death–associated genes were mostly upregulated. Promoters for cell death pathway, death receptor 5, cyclins A1 and C, and caspases-1, -3, and -9, were upregulated, whereas cell death inhibitors, acetyl-CoA transporter, and NF-κB were also upregulated. Moreover, neuroprotective neurotrophic factors such as ciliary neurotrophic factor (CNTF), Hepatocyte growth factor (HGF), and glial cell line–derived neurotrophic factor were upregulated. Inflammation-related genes, such as those belonging to the cytokine family, were not, however, significantly upregulated in either motor neurons or ventral horns. The motor neuron–specific gene expression profile in sporadic ALS can provide direct information on the genes leading to neurodegeneration and neuronal death and are helpful for developing new therapeutic strategies.

Ann Neurol 2005;57:236–251

Amyotrophic lateral sclerosis (ALS) is a devastating neurodegenerative disease characterized by loss of motor neurons in the spinal cord, brainstem, and motor cortex.[1] Initial symptoms include weakness of the limbs, abnormalities of speech, and difficulties in swallowing. The weakness ultimately progresses to complete paralysis, and half of the patients die within 3 years after the onset of symptoms, mostly because of respiratory failure. Approximately 10% of all ALS patients show familial traits, and 20 to 30% of familial ALS patients are associated with a mutation in the copper/zinc superoxide dismutase 1 gene (SOD1). However, more than 90% of ALS patients are sporadic, not showing any familial trait. The presence of Bunina bodies in the remaining spinal motor neurons is a hallmark of sporadic ALS cases.[2,3] So far, several hypotheses about the pathogenesis of sporadic ALS have been proposed based on extensive research on sporadic ALS: oxidative stress, glutamate excitotoxicity, impaired axonal transport, mitochondrial dysfunction, neurotrophic deprivation, proteasomal dysfunction, neuroinflammation, autoimmunity, viral infection, and others.[4–11] Nevertheless, the actual pathogenic mechanism of the selective motor neuron degeneration and ultimate cell death in sporadic ALS remains unknown. There have been extensive studies using animal models and culture systems for familial ALS, especially with SOD1 mutations, but no similar approach is available for studying sporadic ALS.

Recently advances in DNA microarray technology make it possible to analyze global gene expression profiles of thousands of genes in normal as well as pathological tissues. Global gene expression studies using DNA microarray technology have generated valuable

From the [1]Department of Neurology, Nagoya University Graduate School of Medicine, Nagoya; [2]Department of Internal Medicine, Aichi Medical University School of Medicine; and [3]Department of Neuropathology, Institute for Medical Science of Aging, Aichi Medical University School of Medicine, Nagakute, Aichi, Japan.

Received Sep 7, 2004, and in revised form Oct 22. Accepted for publication Nov 14, 2004.

Published online Jan 26, 2005, in Wiley InterScience (www.interscience.wiley.com). DOI: 10.1002/ana.20379

Address correspondence to Dr Sobue, Department of Neurology, Nagoya University Graduate School of Medicine, Nagoya 466-8550, Japan. E-mail: sobueg@med.nagoya-u.ac.jp

 © 2005 American Neurological Association
Published by Wiley-Liss, Inc., through Wiley Subscription Services

information about cell behavior in tissues consisting of homogeneous cell types, cultured cells, and cancer tissues of monoclonal origin.[12,13] In the case of neuronal tissues, particularly those of patients with neurological diseases, however, the complexity of tissues containing multiple lineages of cells, such as neurons, glial cells, and vascular tissues, places limitations on the use of DNA microarray technology. In the lesions of ALS spinal cords, there are reduced numbers of motor neurons with glial cell proliferation, making it difficult to examine motor neuron–specific gene expression.

Laser-captured microdissection (LCM) has been reported to make it possible to isolate single individual neurons from neural tissues with well-preserved mRNA quality.[14,15] In addition, RNA amplification techniques preserving the relative amounts of individual mRNAs have been developed recently.[16,17] LCM and RNA amplification combined with DNA microarray analyses have been reported to enable studies of cell type–specific gene expression profiles in tissues with multiple cell lineages.[16,18] Such integrated analysis system provide an effective tool for investigating the cellular events affecting cell type–specific gene expression profiles in neurodegenerative diseases such as ALS. Indeed, we and other groups demonstrated that these integrated systems could be applied successfully to describe cell-specific gene expression profiles in neuronal tissues.[15,18]

In this study, we applied integrated LCM, RNA amplification, and DNA microarray analysis to clarify alterations of motor neuron–specific gene expression in sporadic ALS cases and successfully obtained expression gene database in situ from degenerating motor neurons in sporadic ALS spinal cord.

Patients and Methods

Tissues from Amyotrophic Lateral Sclerosis and Control Patients

Fresh specimens of lumbar spinal cord (L4 to L5 segment) from 14 sporadic ALS patients (nine men, five women) and 13 neurologically normal patients (nine men, four women) were obtained at autopsy (Table 1). Diagnosis of ALS was

Table 1. Details of Patients Examined in This Study

Patients	Sex	Age (yr)	Duration of Illness (yr)	Postmortem Delay (hr)	Diseases	Spinal Cord Neuropathology Motor Neuron Loss/Gliosis
ALS1	M	72	3.7	6	ALS (B, UL, LL)	Moderate/mild
ALS2	M	71	2.3	5	ALS (LL, UL)	Moderate/mild
ALS3	M	58	1.8	13	ALS (UL, LL, B)	Severe/severe
ALS4	M	43	2.6	5	ALS (LL, B)	Moderate/mild
ALS5	M	53	2.8	11	ALS (B, UL, LL)	Moderate/severe
ALS6	F	79	4.0	4	ALS (UL, LL, B)	Severe/severe
ALS7	F	59	2.5	3	ALS (UL)	Mild/mild
ALS8	F	67	2.0	7	ALS (UL, B)	Severe/mild
ALS9	M	74	4.3	10	ALS (LL, B)	Severe/mild
ALS10	F	47	1.8	4	ALS (B, UL, LL)	Mild/mild
ALS11	M	74	4.5	12	ALS (UL, LL)	Moderate/mild
ALS12	M	57	3.5	5	ALS (LL, UL)	Severe/mild
ALS13	F	53	3.0	8	ALS (B, UL, LL)	Severe/severe
ALS14	M	63	2.2	5	ALS (UL, B)	Mild/mild
Control1	M	57	—	7	Pneumonia	No
Control2	M	78	—	10	Cerebral infarction	No
Control3	M	72	—	9	Lung cancer	No
Control4	F	52	—	7	Pneumonia	No
Control5	F	65	—	12	Pneumonia	No
Control6	M	75	—	10	Heart failure	No
Control7	M	42	—	5	Heart failure	No
Control8	F	76	—	5	Pancreas cancer	No
Control9	F	84	—	6	Myocardial infarction	No
Control10	M	48	—	13	Heart failure	No
Control11	M	77	—	11	Heart failure	No
Control12	M	66	—	11	Cerebral infarction	No
Control13	M	75	—	4	Pneumonia	No

The age, duration of illness, and postmortem delay are indicated for the ALS and control cases. Predominant clinical features of ALS are shown: UL = upper limbs; LL = lower limbs; B = bulbar. Neuropathological involvement of spinal cords was graded as previously. Ten ALS samples were used for microarray analysis: five of them (1, 7, 10, 11, and 14) were analyzed using 4.8K array for spinal motor neurons; five (2, 4, 5, 8, and 12) using 1.0K for spinal motor neurons; five (1, 3, 10, 13, and 14) using 4.8K for spinal ventral horn gray matter; and five (1, 2, 4, 5, and 13) and five (1, 2, 7, 8, and 10) control samples using 4.8K and 1.0K. Thirteen ALS (1–13) and 11 (1–11) control samples were used for TaqMan reverse transcription polymerase chain reaction analysis. Five ALS (1, 10, 11, 13, and 14) and four control (1, 3, 5, and 12) samples were used for in situ hybridization and immunohistochemistry.
ALS = amyotrophic lateral sclerosis.

confirmed by El Escorial diagnostic criteria defined by the World Federation of Neurology and the histopathological findings, particularly the presence of the Bunina body.[2,3] All cases of ALS were sporadic and did not show any heredity. ALS patients with *SOD1* mutation were excluded. The collection of tissues and their use for this study were approved by the ethics committee of Nagoya University Graduate School of Medicine. Tissues were frozen immediately and stored at −80°C until use. The mean ages and standard deviations for ALS and control patients were 62.1 ± 11.0 and 66.7 ± 13.1 years, and the mean postmortem intervals and standard deviations were 7.0 ± 3.3 and 8.5 ± 3.0 hours, respectively. The differences between the means of either age or postmortem interval were not significant between the ALS and control groups. The cause of death in all ALS patients was respiratory failure, and the causes in the control patients were pneumonia, lung cancer, or acute heart failure (see Table 1). Parts of the lumbar spinal cord were fixed in 10% buffered formalin solution, and processed for paraffin sections. The sections were stained with hematoxylin and eosin and Klüver-Barrera and Holzer techniques, and histological assessment was performed. The degree of motor neuron loss and astrogliosis was ranked as mild, moderate or severe according to previously reported.[19,20]

Laser-Captured Microdissection of Spinal Motor Neurons

Sections (10μm) were cut with a standard cryostat, mounted on poly-L-lysin coated slides (Zeiss, Thornwood, NY), and stained with hematoxylin to identify the motor neurons located in the medial and lateral nuclei of the ventral horns of lumber spinal cords. After staining with hematoxylin, the sections were washed in RNase-free water and dried.[21,22] The PALM Robot-Microbeam system (P.A.L.M. Mikrolaser Technology AG, Bernried, Germany) was used for laser capture. The pulsed laser microbeam cut precisely around the targeted motor neurons in the spinal ventral horn (LCM; see Fig 1A–C). The identity of motor neurons was ascertained by reverse transcription polymerase chain reaction (RT-PCR) for choline acetyltransferase (ChAT) as described previously.[15] Each laser-isolated specimen subsequently was ejected from the glass slide with a single or several laser shots and collected directly into the cap of a PCR tube containing denaturing buffer by a process of laser pressure catapulting in the totally noncontact manner previously described.[23] The LCM-isolated cells (approximately 500 pooled cells) were dissolved in denaturing buffer (StrataPrep Total RNA Microprep Kit; Stratagene, San Diego, CA) and stored at −80°C until use.

RNA Extraction of Laser-Captured Microdissection Motor Neuron Samples and Spinal Ventral Horn Homogenates

LCM-isolated cells in denaturing buffer were thawed and centrifuged briefly before the RNA was extracted using a StrataPrep Total RNA Microprep Kit (Stratagene) according to the manufacturer's protocol. RNA was extracted as well from the total homogenates of ventral horn gray matter of spinal cords,[19] which was dissected under a dissecting microscope.

Reverse Transcription and T7 RNA Polymerase Amplification of RNA

Ten microliters of purified RNA obtained as described above was mixed with 1μl of 0.5μg/ml T7-oligodT primer (5′-TCTAGTCGACGGCCAGTGAATTGTAATACGACTCACTATAGGGCGT$_{21}$-3′) to initiate first-strand synthesis. The primer and RNA were incubated in 4μl of 5 × first-strand reaction buffer, 0.1M DTT (2μl), 10mM dNTPs (1μl), 1μl of RNasin, and 1μl of Superscript II reverse transcriptase (Invitrogen, Carlsbad, CA) at 42°C for 1 hour, and then 30μl of 5 × second-strand synthesis buffer, 10mM dNTPs (3μl), 4μl of DNA polymerase, 1μl of *Escherichia coli* RNase H, and 1μl of *E. coli* DNA ligase and 91μl of RNase-free H_2O were added, and the mixture was incubated at 16°C for 2 hours and then at 16°C for 10 minutes after the addition of 2μl of T4 DNA polymerase. Next, an Ampliscribe T7 Transcription Kit (Epicentre Technologies, Madison, WI) was used for RNA amplification: 8μl double-stranded cDNA, 2μl of 10 × Ampliscribe T7 buffer, 1.5μl each of 100mM ATP, CTP, GTP, and UTP, 0.1 M DTT (2μl), and 2μl of T7 RNA polymerase were incubated at 42°C for 3 hours.

For second-round amplification, 10μl of amplified RNA (aRNA) from first-round amplification was mixed together with 1μl of 1mg/ml random hexamers (Invitrogen), and then first-stranded cDNA was synthesized, followed by second-stranded cDNA synthesis as described above. The double-stranded cDNA was subjected to second-round T7 in vitro transcription as above and then subsequent third-round aRNA amplification. After third-round amplification, aRNA was treated with DNase (Wako, Kanagawa, Japan) and cleaned up using an RNeasy Kit (Qiagen, Valencia, CA) according to the manufacturer's protocol.

DNA Microarray Analysis

Fluorescent cDNA probes were synthesized from aRNA of laser-captured spinal motor neurons and RNA from ventral spinal tissue homogenates using an Atlas Glass Fluorescent Labeling Kit (Clontech, Palo Alto, CA) according to the manufacturer's protocol. Cy3-labeled cDNA probes were synthesized from ALS samples for spinal motor neurons and homogenates, and Cy5-labeled cDNA probes were synthesized from control samples. BD Atlas Glass Microarray Human 1.0 and 3.8 (Clontech) slides were hybridized with these fluorescent labeled probes overnight at 50°C and then washed four times and dried according to the manufacturer's protocol. Individual Cy3-labeled cDNA probes from ALS RNA samples of spinal motor neurons and homogenates for each patient were coupled with Cy5-labeled cDNA probes from control RNA samples of those tissues, which were prepared by mixing equal amounts of RNA samples amplified from the control patients. The microarrays were scanned in a laser scanner (GenePix 4000; Axon Instruments, Union City, CA), and the resulting signals were quantified and stored using GenePix Pro analysis software (Axon Instruments). The data for each expressed gene obtained from microarray analysis were expressed as the ratios of the values of individual ALS patients or the means of the values of ALS to the values of the control patients. The values of gene expression levels were means-calculated from motor neurons of 5 or 10 inde-

pendent individuals with ALS as well as from spinal ventral horns of 5 individuals with ALS.

Quantitative Real-Time Reverse Transcription Polymerase Chain Reaction

The probe and primers for the real-time PCR were designed using Primer3′ (S. Rozen and H. J. Skaletsky, available at http://www-genome.wi.mit.edu/genome_software/other/primer3.html). TaqMan PCR was conducted using an iCycler system (Bio-Rad Laboratories, Hercules, CA) with a QuantiTect Probe PCR Kit (Qiagen) and the cDNA according to the manufacturer's protocol. The reaction conditions were 95°C for 3 minutes and then 50 cycles of 15 seconds at 95°C followed by 60 seconds at 55°C. All experiments were performed in quadruplicate, and several negative controls were included. For an internal standard control, the expression of glyceraldehyde-3-phosphate dehydrogenase (GAPDH) was simultaneously quantified. The primers and probe sequences for the examined genes (acetyl-CoA transporter: D88152; Bak: NM_001188; CRABP1: NM_004378; cyclin C: M74091; dynactin 1: NM_004082; EGR3: NM_004430; ephrin A1: M57730; GAPDH: NM_002046; KIAA0231: D86984; and TrkC: U05012) were described in the legends for Figure 3. The threshold cycles of each gene were determined as the number of PCR cycles at which the increase in reporter fluorescence reached 10 times above the baseline signal. The weight ratio of the target gene to GAPDH gives the standardized expression level.

In Situ Hybridization

Frozen sections (10μm thick) of the spinal cord were prepared and immediately fixed in 4% paraformaldehyde. Then, they were treated with 0.1% diethylpyrocarbonate (DEPC) twice for 15 minutes and prehybridized at 45°C for 1 hour. Digoxigenin-labeled cRNA probes were generated from linearized plasmids for the genes of interest using SP6 or T7 polymerase (Roche Diagnostics, Basel, Switzerland). Gene names, Genebank accession number, probe position (nucleotide number), and probe size were as follows: acetyl-CoA transporter, D88152, nucleotides 397-741, 345bp; Bak, NM_001188, nucleotides 792–2094, 345bp; CRABP1, NM_004378, nucleotides 210–545, 336bp; dynactin 1, NM_004082, nucleotides 2392–2774, 383bp; DR5, NM_004082, nucleotides 682–1070, 389bp; EGR3, NM_004430, nucleotides 1433–1794, 362bp; KIAA0231, D86984, nucleotides 698–1053, 356bp; TrkC, U05012, nucleotides 1412–1721, 310bp. After prehybridization, the sections were hybridized with each digoxigenin-labeled cRNA probe overnight at 45°C. The washed sections were incubated with alkaline phosphatase-conjugated anti–digoxigenin antibody (Roche Diagnostics). The signal was visualized with NBT/BCIP (Roche Diagnostics).

Immunohistochemistry

Frozen sections (10μm thick) of the spinal cord were prepared and immediately fixed in 4% paraformaldehyde. Then, they were blocked with 2% bovine serum albumin (Sigma) in Tris-buffered saline at room temperature for 20 minutes and incubated with anti–cyclin C (1:200 dilution; Santa Cruz Biotechnology, Santa Cruz, CA) antibody overnight at 4°C. Subsequent procedures were performed using ENVISION++KIT/HRP (diaminobenzidine tetrahydrochloride; DAKO, Carpinteria, CA) according to the manufacturer's protocol.

Statistical Analyses

To assess the correlation of intensity values for each labeling sample, we used scatterplots and measured linear relationships. The correlation coefficient, R^2, that was calculated indicates the variability of intensity values between Cy-5– and Cy-3–labeled samples. To perform cluster analyses of hierarchical clustering, self-organizing maps (SOM) and principal component analysis after logarithmic transformation, we used Acuity 3.0 software (Axon Instruments). The data measured by quantitative real-time RT-PCR analysis were analyzed by Student's t tests.

Results

T7 Amplification Preserves Gene Expression Profiles

Because the amounts of laser-microdissected samples were extremely low and did not contain enough mRNA for further analysis, RNA amplification was required. It was critical to achieve sufficient RNA amplification and yet maintain the expression profiles of mRNAs. We performed experiments to determine how the expression profiles of mRNAs were affected by the T7 amplification procedure. RNA samples were extracted from control spinal cords and a part of RNA samples was amplified using T7 amplification. One flourescently labeled probe was synthesized from an individually amplified RNA (aRNA) or nonamplified RNA (nRNA) and was hybridized to microarrays. Independent amplification of RNA yielded quite similar expression patterns. The correlation of signal intensities between independent amplifications for the third aRNA was $R^2 = 0.9157$, $p < 0.0001$, and on the other hand, the correlation of signal intensities in nRNA was $R^2 = 0.9157$, $p < 0.0001$ (Fig 1D, E). Previous reports using similar amplification procedures as ours also have confirmed the reproducibility of T7 amplification for the preservation of RNA expression profiles.[14,15,17] In this study, the third-round amplification was performed for the LCM-isolated motor neurons, but for the spinal ventral horn homogenates a single amplification produced enough RNA for further analysis, and similar expression patterns were found between the first and third amplifications (data not shown).

Gene Expression Database of Spinal Motor Neurons and Ventral Horn Homogenates of Amyotrophic Lateral Sclerosis

aRNA samples from the motor neurons and the ventral horn homogenates from the lumbar spinal cords were subjected to microarray analysis. The differences of the gene expression levels between ALS and control sam-

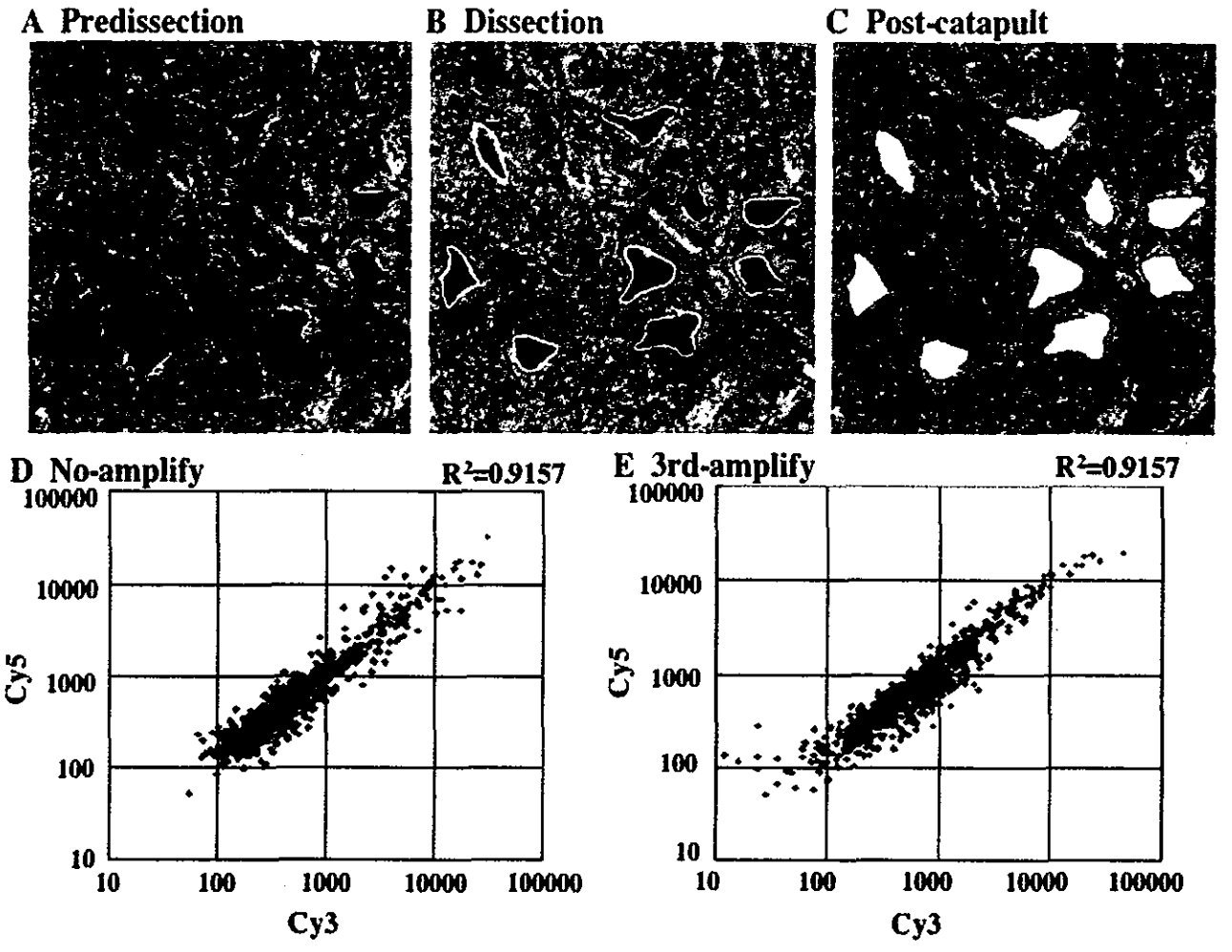

Fig 1. Verification of laser-captured microdissection (LCM) and RNA amplification. Microdissection of motor neurons in spinal ventral horn: sections were stained with hematoxylin (A); margins of motor neurons were dissected by the laser beam (B); and motor neurons were isolated from slides by laser pressure catapulting (C). Scatterplots of nonamplified and amplified RNAs: correlations between independent amplifications of control spinal cord samples are shown using nonamplified (D) and third amplified RNAs (E). These RNAs were split into two samples for labeling of Cy5 and Cy3 and hybridized separately to two microarrays. The very high squared correlations reflect the high reproducibility of the hybridization results with the same values between nonamplified and third amplified RNAs.

ples were expressed as ratios of the values of ALS individuals compared with the mean values of the controls. One percent (52/4,845) of genes examined were significantly upregulated in spinal motor neurons of ALS patients and 3% (144/4,845) were downregulated, assuming that the changes of 3.0-fold increase and 0.3-fold decrease were significant, when the mean levels of gene expression were calculated. In contrast with motor neurons, the total spinal ventral horn homogenates demonstrated 0.7% (37/4,845) and 0.2% (8/4,845) significant upregulation and downregulation of gene expression, respectively.

The genes prominently altered in ALS are listed in Tables 2 to 5 for spinal motor neurons and spinal ventral horn homogenates, respectively. Several upregulated genes listed were overlapping between spinal motor neurons (see Table 2) and ventral horns (see Table 4), suggesting that motor neuron overexpression is reflected to some extent by gene expression in ventral horn homogenates. The other genes upregulated in motor neurons were not present in the list for spinal ventral horns, because these gene expression changes were diluted and masked by changes occurring in other cell types. Because the number of spinal motor neurons was decreased in ALS spinal cords, most genes that were listed as downregulated genes in motor neurons (see Table 3) were not found in spinal ventral horns (see Table 5) except for three genes (CRABP1, EGR3, and postmeiotic segregation increased 2-like 11). When we categorized these altered genes in ALS motor neurons into several functional groups, the genes related to cell receptors and intracellular signaling, transcription,

Table 2. Upregulated Genes in ALS Motor Neurons (Top 30)

GeneBank No.	Gene Name	Fold Change (ALS/control)
NM_003419	Zinc finger protein 10 (KOX 1)	8.86
U91618	Neurotensin/neuromedin N precursor	8.33*
NM_004651	Ubiquitin-specific protease 11	8.13
D86984	KIAA0231	7.31*
A26792	Ciliary neuronotrophic factor (CNTF)	6.76
M77830	Desmoplakin I & II (DSP; DPI & DPII)	6.10
NM_005622	SA (rat hypertension-associated) homolog	5.47
NM_004733	Acetyl-coenzyme A transporter	5.33
NM_000021	Presenilin 1 (Alzheimer disease 3)	4.96
K03020	Phenylalanine-4-hydroxylase (PAH)	4.95*
AF016268	Death receptor 5 (DR5); cytotoxic TRAIL receptor, TNFR10b	4.91*
M74091	G1/S-specific cyclin C (CCNC)	4.82*
NM_000275	Oculocutaneous albinism II	4.78
AF000936	SH3-binding protein 2	4.73*
NM_000384	Apolipoprotein B	4.70
M63099	Interleukin-1 receptor antagonist	4.66*
M57730	Ephrin-A1	4.57*
L19067	NF-κ B transcription factor p65 subunit	4.52*
U66838	Cyclin A1 (CCNA1)	4.51*
NM_005021	Ectonucleotide pyrophosphatase/phosphodiesterase 3	4.48
NM_001550	Interferon-related developmental regulator 1	4.45
L25851	Integrin alpha E precursor (ITGAE)	4.43*
X16416	C-abl1 protooncogene	4.41
U08015	Transcription factor NF-ATc	4.40*
U44378	Mothers against dpp homolog 4 (SMAD4)	4.35*
NM_005067	Seven in absentia (Drosophila) homolog 2	4.22
J04536	Leukosialin precursor; sialophorin	4.19*
X06745	DNA polymerase alpha catalytic subunit	4.15*
U09564	Serine kinase	4.09*
U37139	β 3-endonexin	4.06*

Gene expression levels are expressed as means of fold-change, which is calculated by dividing the signals of each ALS sample by those of control samples, in the 5 or 10 (denoted by asterisk) patients with ALS.
ALS = amyotrophic lateral sclerosis.

metabolism, and cytoskeletal architecture were downregulated. The functional categories of secreted and extracellular communication proteins and cell cycle regulators were characteristically upregulated. A complete list of the differentially expressed genes is available online at http://www.med.nagoya-u.ac.jp/neurology/index.html.

Differential Gene Expression Profiles between Spinal Motor Neurons and Ventral Horn Homogenates of Amyotrophic Lateral Sclerosis

To compare the expression profile of motor neurons with that of spinal ventral horn homogenates, we performed cluster analyses. Because the patterns of gene expression from microarray analysis are impossible to discern by eye, data analysis software (Acuity 3.0 software; Axon Instruments) was used based on the dimensionality of the data: hierarchical clustering for high dimensional gene space and principal component analysis and SOM for low one. Hierarchical clustering clearly discriminated the expression profile of isolated motor neurons from that of ventral horn homogenates, showing two grouped branches of the dendrogram with a correlation coefficient of 0.446 (Fig 2A). Moreover, a principal component analysis confirmed the distinction of gene expression profiles between spinal motor neurons and ventral horns (see Fig 2B). The gene expression profile of motor neurons was clustered into a single cluster by the two clustering algorithms, which was well separated from that of spinal ventral horn gray matter, suggesting a relatively uniform degenerating process in spinal motor neurons in ALS.

Motor Neuron–Specific Gene Expression Profiles Identified by the Self-Organizing Map Analysis

To further analyze the expression pattern specific to spinal motor neurons, a SOM was produced as a nonhierarchical clustering.[24,25] The examined genes were subdivided into 25 clustered categories, and the selected genes are shown in a certain group of the SOM (see Fig 2C, Table 6). The genes contained in the clusters reflect the expression pattern in spinal motor neurons as well as that in spinal ventral horns, and these selected genes are somehow different from those in Tables 2 to 5 because of the different bases of classification. Clustering of the SOM showed motor neu-